

# Strongly Magnetically Tuned Exciton-Polaritons in van der Waals CrSBr

Chun Li,<sup>1,†</sup> Chao Shen,<sup>2,3,†</sup> Xuekai Ma,<sup>4</sup> Nai Jiang,<sup>2</sup> Jiepeng Song,<sup>1</sup> Kwok Kwan Tang,<sup>1</sup> Xinyi Deng,<sup>1</sup> Jiaqi Guo,<sup>2</sup> Xinfeng Liu,<sup>5</sup> and Qing Zhang<sup>1,\*</sup>

<sup>1</sup>School of Materials Science and Engineering, Peking University, Beijing 100871, China

<sup>2</sup>State Key Laboratory for Superlattices and Microstructures, Institute of Semiconductors, Chinese Academy of Sciences, Beijing 100083, China

<sup>3</sup>Center of Materials Science and Optoelectronics Engineering, University of Chinese Academy of Sciences, Beijing 100049, China

<sup>4</sup>Department of Physics and Center for Optoelectronics and Photonics Paderborn (CeOPP), University of Paderborn, Warburger Strasse 100, 33098 Paderborn, Germany

<sup>5</sup>CAS Key Laboratory of Standardization and Measurement for Nanotechnology, CAS Center of Excellence for Nanoscience, National Center for Nanoscience and Technology, Beijing 100190, China

\*Q\_zhang@pku.edu.cn

†These authors contributed equally to this work.

## Abstract

2D van der Waals (vdW) magnetic semiconductors offer an ideal platform to achieve exciton-polaritons correlated with magnetic orders for developing solid-state quantum, spintronic, and photonic devices. However, in the as-demonstrated systems, the coupling strength, light velocity, and effective mass of exciton-polaritons are almost inert to the external magnetic field. Here, we report the experimental observation of giant magnetic tuning of B exciton-polaritons in vdW magnet CrSBr crystals. The Rabi splitting energy is tuned up to 100 meV within a moderate 0.45 T in-plane magnetic field due to changes in excitonic states during the spin transitions. Besides, the light velocity and effective mass of exciton-polaritons are tuned by 10.3% and 26.1% below 100 meV of exciton energy. Further, the strong coupling persists at room temperature, controlled by temperature-tailored exciton-magnon and exciton-phonon coupling. These results advance the development of on-demand strong coupling systems for spin-correlated quantum optoelectronic applications.

## 1. Introduction

Strong light-matter coupling plays a pivotal role in modern physics spanning from quantum electrodynamics, nonlinear photonics, ultrafast optics to condensed matter physics.<sup>[1]</sup> In semiconductor excitonic systems, strong exciton-photon coupling gives rise to hybrid exciton-polaritons when the coupling strengths exceed the decay rates of both excitons and photons.<sup>[2]</sup> Exciton-polaritons inherit the strong interaction from the excitonic component and the light effective mass from the photonic component, holding significant promise for numerous technological applications such as low-threshold polariton lasers, all-optical switches, and quantum simulators.<sup>[3-5]</sup> Finding ideal excitonic systems to create exciton-polaritons at ambient conditions continues to attract interest, driving the development of materials from III-V/II-VI quantum wells to ZnO, GaN, organic molecules, and halide perovskites.<sup>[6-13]</sup> In the past decade, the emerging 2D van der Waals (vdW) semiconductors that host large exciton binding energy and oscillator strength meet the requirements for room-temperature polaritonic applications.<sup>[14-18]</sup> Besides, the weak interlayer interactions in 2D vdW semiconductors allow the flexible exfoliation to the desired thickness (down to sub-nanometer level) and rich stacking engineering, facilitating the coupling with optical microcavities and on-chip integration of large-area polaritonic devices.<sup>[19]</sup>

In particular, magnetic vdW semiconductors serve as crucial bridges connecting strong light-matter physics and magnetic excitations, and investigating their fundamental interplay presents promising opportunities for spintronics and quantum computing.<sup>[20-22]</sup> Magnetic field can provide a new degree of freedom for manipulating strong exciton-photon coupling, as the energy levels and dynamics of magnetic excitons are highly sensitive to the underlying magnetic orders.<sup>[23-26]</sup> Additionally, the strong electronic and spintronic correlation information will be carried by the exciton-polaritons, well-suited for optical detection and transmission.<sup>[27-29]</sup> The strong coupling between magnetic excitons and photons in vdW antiferromagnet NiPS<sub>3</sub> occurred with limited coupling strength (a few meV) and at cryogenic temperatures.<sup>[30]</sup> The band-edge A exciton-photon coupling in vdW antiferromagnet CrSBr exhibited a giant coupling strength, but the magnetic tuning is only effective for exciton-polariton energy at the level of

~15 meV through tuning the intrinsic exciton energy.<sup>[31-33]</sup> Real-time magnetic control of the strong coupling behaviors offers potential for developing programmable quantum polariton systems with on-demand energy landscape, coherence time, and nonlinear interaction, which, however, has been rarely explored.

Here, we report the observation of magnetic field engineering B exciton-photon coupling behaviors in CrSBr crystals through the spin flip transition. We find both remarkably large tuning of exciton-polariton energy (up to 60 meV) and Rabi splitting energy (up to 100 meV) during the antiferromagnetic (AFM) to ferromagnetic (FM) order change. The resulting modulation of light velocity and effective mass of exciton-polaritons 100 meV apart at the low-energy side of B exciton is 10.3% and 26.1%, respectively. Furthermore, temperature can mediate the coupled exciton-polariton behaviors by manipulating the interactions between excitons and magnons/phonons, hosting strong coupling up to room temperature. These results pave the way for achieving controllable strong coupling in polaritonic optoelectronics and quantum applications.

## 2. Results and Discussion

We focus on the high energy exciton around 1.8 eV (B exciton) in CrSBr, attributed to the direct transition from the second valence band to the second conduction band at the Brillouin  $\Gamma$  point (Figure 1a). Mesoscopic CrSBr crystals, with thicknesses ranging from tens to hundreds of nanometers, were prepared using mechanical and transferred onto the SiO<sub>2</sub>/Si substrate. The elongated morphology of the crystals reflects the anisotropic lattice structure of the material (Figure 1b). To probe the excitonic resonance, we investigated two types of optical contrasts from differential reflectance spectroscopy and magnetic circular dichroism (MCD) spectroscopy. In both experiments, the temperature was maintained at 80 K, with the magnetic structure of CrSBr in a field-induced FM state achieved by applying a specific external magnetic field to ensure the consistency of the exciton states. Polarization-resolved reflectance spectra indicate a reflectance dip at 1.764 eV as the polarization of the reflected light is along the *a*-axis, assigned to an uncoupled cavity mode (Figure 1c). In contrast, when the polarization

is along the  $b$ -axis, a series of reflectance dips below 1.8 eV varying with the crystal thickness exist (Figure S1), suggesting the presence of exciton-polaritons (discussed in the subsequent section). Two representative exciton-polariton signals at 1.654 eV and 1.593 eV can be identified in both the differential reflectance spectra and MCD spectra, providing a consistency check of exciton-related absorption (Figure 1d). The polarization nature of the uncoupled cavity mode and coupled exciton-polaritons is independent of temperature and magnetic field (Figure S2). Figure 1e presents angle-resolved reflectance spectra for a 354 nm-thick CrSBr crystal taken at 6 K (298 K) without the external magnetic field, with a maximum detection angle of approximately  $\pm 26^\circ$  ( $\pm 64^\circ$ ). The angle-resolved spectrum at 6 K exhibits three curved dispersions, well fitted using an exciton-polariton model with a Rabi splitting energy of 632 meV. The normalized coupling strength of 0.177 reveals the demonstration of ultrastrong exciton-photon coupling, dramatically exceeding that of the reported self-hybridized exciton-polariton systems. The larger dispersion curvature and increased linewidth in the lower branches indicate a reduction in effective mass and an increase in dissipation with the mixing of more photons. Due to phonon-assisted exciton linewidth broadening, only two exciton-polariton branches are observed at room temperature, with a fitted Rabi splitting energy of 780 meV.

Next, we measured the reflectance dip energy at normal incidence in CrSBr crystals of different thicknesses and extracted the effective refractive index  $n_{\text{eff}}$ , regarding the out-of-plane Fabry–Pérot resonance (Note S1). When the polarization of reflected light is along the  $b$ -axis, the  $n_{\text{eff}}$  sharply increases as energy approaches 1.8 eV (Figure 2a). This obvious increase exceeds the refractive index variation described by the Sellmeier equation, extracted from the data when the polarization is along the  $a$ -axis (without exciton effect), indicating the occurrence of strong exciton-photon coupling. The fitted exciton oscillator strength reaches  $7.28 \text{ (eV)}^2$ , which is around four times greater than that of the band-edge A exciton.<sup>[31-33]</sup> Additionally, we used a coupled oscillator model to quantitatively fit the energy-wavevector dispersion showing anti-crossing features (Figure 2b and Note S2). The fitted average Rabi splitting energy reaches 695 meV, much larger than the average dissipation energy of excitons ( $\sim 50$  meV) and photons ( $\sim 50$

meV), confirming the formation of exciton-polaritons.

Pronounced nonlinearity is another key feature of exciton-polaritons. Figure 2c shows the representative reflectance spectra of three exciton-polariton branches in the 354 nm-thick crystal at different excitation densities. As excitation density increases, all branches exhibit a linear blueshift, and the absolute value of the blueshift progressively increases as the exciton component decreases (Figure 2d). Within the excitation density range of interest, the fitted exciton energy almost remains unchanged, reflecting the suppressed long-range excitonic interactions (Figure 2e). Similar behavior has been reported in other zero-dimensional and one-dimensional exciton systems with highly localized wavefunctions.<sup>[15, 30]</sup> Due to the Pauli exclusion principle, the Rabi splitting energy saturates as the excitation density approaches the fitted saturation exciton density at  $1.52 \times 10^{14} \text{ cm}^{-2}$  (Note S3). Considering the anisotropic dielectric function and the elliptical distribution of the exciton wavefunction, the predicted B exciton Bohr radius along the *b*-axis and *a*-axis is 0.90 nm and 0.25 nm, respectively. The consistency of these results indicates that the strongly localized nature of excitons leads to the extremely large exciton oscillator strength and thus the occurrence of ultrastrong coupling.

The behaviors of B exciton and B exciton-polaritons are highly dependent on the magnetic order and can be effectively tailored by an applied external magnetic field. At 6 K, reflectance spectra at normal incidence as a function of the in-plane magnetic field (parallel to the easy *b*-axis) show that all exciton-polariton branches maintain the constant energies when *B* is less than 0.35 T, followed by an abrupt redshift between 0.35-0.45 T, after which the energies stabilize again as *B* exceeds 0.45 T (Figure 3a and 3b). This sudden redshift arises from changes in interlayer electronic hybridization due to spin flipping, accomplished by the transition from AFM to FM order.<sup>[24]</sup> Interestingly, the Rabi splitting energy also sharply decreases from 632 meV to 535 meV across the spin flipping transition (Figure 3c). In contrast, the Rabi splitting energy for the coupling of A excitons and photons is almost independent of the magnetic order (Figure S3). Therefore, the resulting modulation of light velocity and effective mass of exciton-polaritons 100 meV below the B exciton energy reach 10.3% and 26.1%, 1-2 orders of magnitude higher than those of A exciton-polariton (Figure S4 and Note S4). Further, the fitted

energy redshift of B exciton is  $\sim 78$  meV, nearly five times that of A exciton ( $\sim 16$  meV, Figure S5), reflecting dramatic field-induced band structure change associated with the B exciton transition. The reduced coupling strength will decrease the global vacuum energy in the ultrastrong coupling system, confirmed by the fact that the direct measured energy shift of B exciton in a few-layer sample without exciton-polaritons,  $\sim 88$  meV (Figure S6), is higher than the fitted value ( $\sim 78$  meV) using strong coupling model. When the temperature increases to 80 K, similar switching behaviors in exciton-polariton energy, Rabi splitting energy, and B exciton energy are observed (Figure 3d-3f and S5). The critical magnetic field for the spin flipping transition is lower ( $\sim 0.15$ - $0.20$  T), above which a slight energy redshift still occurs. These results are due to thermal fluctuations weakening the pristine AFM coupling and field-induced FM coupling.<sup>[33]</sup> At 150 K (above the Néel temperature of 132 K for bulk CrSBr), CrSBr transforms into a paramagnetic state, and the magnetic response of both B excitons and B exciton-polaritons vanishes completely (Figure 3g-3i and S5).

MCD spectroscopy was employed to further verify the magnetic tuning of ultrastrong coupling. Figure 3j presents the out-of-plane magnetic field (parallel to the hard  $c$ -axis) dependence of MCD spectra at 80 K. The exciton-polariton branches exhibit a continuous redshift with increasing magnetic field (Figure 3k), consistent with the spin canting process. The redshift rate slows down significantly at  $B > 1$  T, accompanied by saturation of the MCD intensity growth (Figure S7), highlighting the critical magnetic field strength for the AFM-FM phase transition. Similarly, fitted Rabi splitting energy and B exciton energy also continuously undergo a reduction and gradually stabilize beyond  $B$  of 1 T (Figure 3l and S5). The consistency between the reflectance and MCD spectra at the same temperature of 80 K, across both AFM and FM phases, verifies the reliability of the data.

Temperature dependence of reflectance spectra was collected to unlock the evolution of exciton-polaritons influenced by excitons interacting with incoherent magnons and phonons (Figure 4a and S8). As  $B = 0$  T, all exciton-polariton branches monotonically redshift below 100 K, and transform to blueshift between 100 and 200 K. As  $B = 1$  T (above the critical field for the AFM-FM transition), an accelerated blueshift occurs below 200 K, resulting in a

continuous reduction of field-induced energy shift  $E_{\text{shift}}$  for both exciton-polaritons and excitons until  $\sim 140$  K (Figure 4b). The trend of  $E_{\text{shift}}$  can be well described by the exciton-magnon coupling theory (Note S5), and the fitted surviving temperature for short-range correlations is 141.6 K, consistent with the Néel temperature. Further, the fitted exciton energy in both AFM and FM phases across 6-298 K matches the model considering both magnon- and phonon-related temperature dependence of exciton energy (Figure S9). Specifically, the temperature dependent behaviors of the Rabi splitting energy closely mirror the fitted exciton energy (Figure 4c), where the tunable Rabi splitting decreases from  $\sim 100$  meV ( $\sim 12.8\%$ ) at 6 K to zero above 140 K (Figure S10), suggesting strong spin and phonon correlated exciton-photon coupling (Note S6). The robust ultrastrong coupling up to room temperature (Figure S11), along with significant tunability in coupling strength, light velocity, and effective mass, opens up new possibilities for magnetically responsive exciton-polariton applications in quantum information storage and processing.

### 3. Conclusion

In summary, the exceptionally large magnetically tunable Rabi splitting energy ( $\sim 100$  meV), light velocity ( $\sim 10.3\%$ ), and effective mass ( $\sim 26.1\%$ ) achieved in CrSBr crystals, surpassing most known semiconductor exciton-polaritons systems, makes CrSBr an attractive candidate for future studies in spin-correlated strong light-matter physics. Moreover, the ultrastrong coupling surviving up to room temperature in an open cavity, combined with the rich stacking engineering of vdW materials, offers an ideal platform for chip-level integrated polaritonic devices that interconnect magnetic, electronic, and photonic functionalities, with potential applications in non-volatile memory, quantum computing, and magneto-optical detection.

### 4. Experimental Section

**Sample preparations.** The CrSBr crystals were mechanically exfoliated from the bulk single crystal (purchased from Nanjing MKNANO Tech. Co., Ltd.) using Scotch tape and transferred onto the pre-cleaned SiO<sub>2</sub>/Si substrate (SiO<sub>2</sub> thickness: 285 nm).

**Optical characterizations.**

The angle-resolved measurements at room temperature were carried out by using a home-built Fourier imaging setup, where the reflectance (source: halogen lamp) signals were collected through a 100× objective (N.A. = 0.9), then sent to a spectrometer (Horiba, iHR320). Low-temperature measurements were carried out in Montana cryostat (Montana, CR-562), equipped with a 50× objective (N.A. = 0.45) for angle-resolved reflectance, and the spectra were detected using a spectrometer (Horiba, iHR550). The in-plane magnetic field-dependent measurements were realized using an electromagnet (Yingpu Magnetolectric, WD-130). For excitation density dependent spectroscopy, the excitation source was derived from a supercontinuum laser (NKT Photonics, Fianium WhiteLase) with a repetition rate of 80 MHz and a pulse width of 6 ps, which was spectrally filtered using a band-pass filter with controllable tilt angle. In the MCD measurements, the excitation source was a wavelength tunable laser derived from a supercontinuum laser (YSL Photonics, SC-pro) with a repetition rate of 80 MHz and a pulse width of 6 ps, equipped with a monochromator (Horiba, iHR320). The detection of the reflected light from the sample was achieved using a Si photodetector. MCD signals were measured with two lock-in amplifiers, referencing a 177 Hz chopper and a 50 kHz photoelastic modulator. The out-of-plane magnetic field was provided by a superconducting magnet (CryoMagnetics).

### **Supporting Information**

The Supporting Information is available.

### **Acknowledgements**

Q.Z. acknowledges funding support from the National Natural Science Foundation of China (U23A2076, 51991340, 52072006) and the Beijing National Natural Science Foundation (JQ21004). C.S. acknowledges funding support from the National Key Research and Development Program of China (2022YFF1201900).

### **Conflict of Interest**

The authors declare no conflict of interest.

### **Author Contributions**

Q.Z. conceived the idea and led the project. C.L. and K.K.T. fabricated the samples. C.L. and N.J. conducted the optical spectroscopy measurements. C.L. and Q.Z. drafted the manuscript. All the authors discussed the results and revised the manuscript.

## References

- [1] J. Bloch, A. Cavalleri, V. Galitski, M. Hafezi, A. Rubio, Strongly correlated electron–photon systems, *Nature* 2022, **606**, 41.
- [2] J. J. Hopfield, Theory of the Contribution of Excitons to the Complex Dielectric Constant of Crystals, *Physical Review* 1958, **112**, 1555.
- [3] D. Sanvitto, S. Kéna-Cohen, The road towards polaritonic devices, *Nature Materials* 2016, **15**, 1061.
- [4] A. Kavokin, T. C. H. Liew, C. Schneider, P. G. Lagoudakis, S. Klemmt, S. Hoefling, Polariton condensates for classical and quantum computing, *Nature Reviews Physics* 2022, **4**, 435.
- [5] J. Bloch, I. Carusotto, M. Wouters, Non-equilibrium Bose–Einstein condensation in photonic systems, *Nature Reviews Physics* 2022, **4**, 470.
- [6] H. Deng, G. Weihs, C. Santori, J. Bloch, Y. Yamamoto, Condensation of Semiconductor Microcavity Exciton Polaritons, *Science* 2002, **298**, 199.
- [7] J. Kasprzak, M. Richard, S. Kundermann, A. Baas, P. Jeambrun, J. M. J. Keeling, F. M. Marchetti, M. H. Szymańska, R. André, J. L. Staehli, V. Savona, P. B. Littlewood, B. Deveaud, L. S. Dang, Bose–Einstein condensation of exciton polaritons, *Nature* 2006, **443**, 409.
- [8] H. Li, F. Chen, H. Jia, Z. Ye, H. Zhou, S. Luo, J. Shi, Z. Sun, H. Xu, H. Xu, T. Byrnes, Z. Chen, J. Wu, All-optical temporal logic gates in localized exciton polaritons, *Nature Photonics* 2024, **18**, 864.
- [9] S. Christopoulos, G. B. H. von Högersthal, A. J. D. Grundy, P. G. Lagoudakis, A. V. Kavokin, J. J. Baumberg, G. Christmann, R. Butté, E. Feltin, J. F. Carlin, N. Grandjean, Room-Temperature Polariton Lasing in Semiconductor Microcavities, *Physical Review Letters* 2007, **98**, 126405.
- [10] A. V. Zasedatelev, A. V. Baranikov, D. Sannikov, D. Urbonas, F. Scafirimuto, V. Y. Shishkov, E. S. Andrianov, Y. E. Lozovik, U. Scherf, T. Stöferle, R. F. Mahrt, P. G. Lagoudakis, Single-photon nonlinearity at room temperature, *Nature* 2021, **597**, 493.
- [11] J. Liang, W. Wen, F. Jin, Y. G. Rubo, T. C. H. Liew, R. Su, Polariton spin Hall effect in a Rashba–Dresselhaus regime at room temperature, *Nature Photonics* 2024, **18**, 357.

- [12]X. Wu, S. Zhang, J. Song, X. Deng, W. Du, X. Zeng, Y. Zhang, Z. Zhang, Y. Chen, Y. Wang, C. Jiang, Y. Zhong, B. Wu, Z. Zhu, Y. Liang, Q. Zhang, Q. Xiong, X. Liu, Exciton polariton condensation from bound states in the continuum at room temperature, *Nature Communications* 2024, **15**, 3345.
- [13]J. Song, Q. Shang, X. Deng, Y. Liang, C. Li, X. Liu, Q. Xiong, Q. Zhang, Continuous-Wave Pumped Perovskite Lasers with Device Area Below 1  $\mu\text{m}^2$ , *Advanced Materials* 2023, **35**, 2302170.
- [14]W. Liu, Z. Ji, Y. Wang, G. Modi, M. Hwang, B. Zheng, V. J. Sorger, A. Pan, R. Agarwal, Generation of helical topological exciton-polaritons, *Science* 2020, **370**, 600.
- [15]L. Zhang, F. Wu, S. Hou, Z. Zhang, Y.-H. Chou, K. Watanabe, T. Taniguchi, S. R. Forrest, H. Deng, Van der Waals heterostructure polaritons with moiré-induced nonlinearity, *Nature* 2021, **591**, 61.
- [16]C. Anton-Solanas, M. Waldherr, M. Klaas, H. Suchomel, T. H. Harder, H. Cai, E. Sedov, S. Klemmt, A. V. Kavokin, S. Tongay, K. Watanabe, T. Taniguchi, S. Höfling, C. Schneider, Bosonic condensation of exciton–polaritons in an atomically thin crystal, *Nature Materials* 2021, **20**, 1233.
- [17]E. Maggiolini, L. Polimeno, F. Todisco, A. Di Renzo, B. Han, M. De Giorgi, V. Ardizzone, C. Schneider, R. Mastria, A. Cannavale, M. Pugliese, L. De Marco, A. Rizzo, V. Maiorano, G. Gigli, D. Gerace, D. Sanvitto, D. Ballarini, Strongly enhanced light–matter coupling of monolayer WS<sub>2</sub> from a bound state in the continuum, *Nature Materials* 2023, **22**, 964.
- [18]T. Wu, C. Wang, G. Hu, Z. Wang, J. Zhao, Z. Wang, K. Chaykun, L. Liu, M. Chen, D. Li, S. Zhu, Q. Xiong, Z. Shen, H. Gao, F. J. Garcia-Vidal, L. Wei, Q. J. Wang, Y. Luo, Ultrastrong exciton-plasmon couplings in WS<sub>2</sub> multilayers synthesized with a random multi-singular metasurface at room temperature, *Nature Communications* 2024, **15**, 3295.
- [19]Y. Luo, J. Zhao, A. Fieramosca, Q. Guo, H. Kang, X. Liu, T. C. H. Liew, D. Sanvitto, Z. An, S. Ghosh, Z. Wang, H. Xu, Q. Xiong, Strong light-matter coupling in van der Waals materials, *Light: Science & Applications* 2024, **13**, 203.
- [20]K. S. Burch, D. Mandrus, J.-G. Park, Magnetism in two-dimensional van der Waals materials, *Nature* 2018, **563**, 47.

- [21]J. T. Gish, D. Lebedev, T. W. Song, V. K. Sangwan, M. C. Hersam, Van der Waals opto-spintronics, *Nature Electronics* 2024, **7**, 336.
- [22]J. F. Sierra, J. Fabian, R. K. Kawakami, S. Roche, S. O. Valenzuela, Van der Waals heterostructures for spintronics and opto-spintronics, *Nature Nanotechnology* 2021, **16**, 856.
- [23]X. Wang, J. Cao, Z. Lu, A. Cohen, H. Kitadai, T. Li, Q. Tan, M. Wilson, C. H. Lui, D. Smirnov, S. Sharifzadeh, X. Ling, Spin-induced linear polarization of photoluminescence in antiferromagnetic van der Waals crystals, *Nature Materials* 2021, **20**, 964.
- [24]N. P. Wilson, K. Lee, J. Cenker, K. Xie, A. H. Dismukes, E. J. Telford, J. Fonseca, S. Sivakumar, C. Dean, T. Cao, X. Roy, X. Xu, X. Zhu, Interlayer electronic coupling on demand in a 2D magnetic semiconductor, *Nature Materials* 2021, **20**, 1657.
- [25]G. M. Diederich, J. Cenker, Y. Ren, J. Fonseca, D. G. Chica, Y. J. Bae, X. Zhu, X. Roy, T. Cao, D. Xiao, X. Xu, Tunable interaction between excitons and hybridized magnons in a layered semiconductor, *Nature Nanotechnology* 2023, **18**, 23.
- [26]F. Song, Y. Lv, Y.-J. Sun, S. Pang, H. Chang, S. Guan, J.-M. Lai, X.-J. Wang, B. Wu, C. Hu, Z. Yuan, J. Zhang, Manipulation of anisotropic Zhang-Rice exciton in NiPS<sub>3</sub> by magnetic field, *Nature Communications* 2024, **15**, 7841.
- [27]H. Y. Yuan, Y. Cao, A. Kamra, R. A. Duine, P. Yan, Quantum magnonics: When magnon spintronics meets quantum information science, *Physics Reports* 2022, **965**, 1.
- [28]P. Pirro, V. I. Vasyuchka, A. A. Serga, B. Hillebrands, Advances in coherent magnonics, *Nature Reviews Materials* 2021, **6**, 1114.
- [29]D. D. Awschalom, C. R. Du, R. He, F. J. Heremans, A. Hoffmann, J. Hou, H. Kurebayashi, Y. Li, L. Liu, V. Novosad, J. Sklenar, S. E. Sullivan, D. Sun, H. Tang, V. Tyberkevych, C. Trevillian, A. W. Tsen, L. R. Weiss, W. Zhang, X. Zhang, L. Zhao, C. W. Zollitsch, Quantum Engineering With Hybrid Magnonic Systems and Materials (Invited Paper), *IEEE Transactions on Quantum Engineering* 2021, **2**, 1.
- [30]F. Dirnberger, R. Bushati, B. Datta, A. Kumar, A. H. MacDonald, E. Baldini, V. M. Menon, Spin-correlated exciton–polaritons in a van der Waals magnet, *Nature Nanotechnology* 2022, **17**, 1060.
- [31]F. Dirnberger, J. Quan, R. Bushati, G. M. Diederich, M. Florian, J. Klein, K. Mosina, Z.

Sofer, X. Xu, A. Kamra, F. J. García-Vidal, A. Alù, V. M. Menon, Magneto-optics in a van der Waals magnet tuned by self-hybridized polaritons, *Nature* 2023, **620**, 533.

[32] T. Wang, D. Zhang, S. Yang, Z. Lin, Q. Chen, J. Yang, Q. Gong, Z. Chen, Y. Ye, W. Liu, Magnetically-dressed CrSBr exciton-polaritons in ultrastrong coupling regime, *Nature Communications* 2023, **14**, 5966.

[33] C. Li, C. Shen, N. Jiang, K. K. Tang, X. Liu, J. Guo, Y. Liang, J. Song, X. Deng, Q. Zhang, 2D CrSBr Enables Magnetically Controllable Exciton-Polaritons in an Open Cavity, *Advanced Functional Materials* 2024, **n/a**, 2411589.

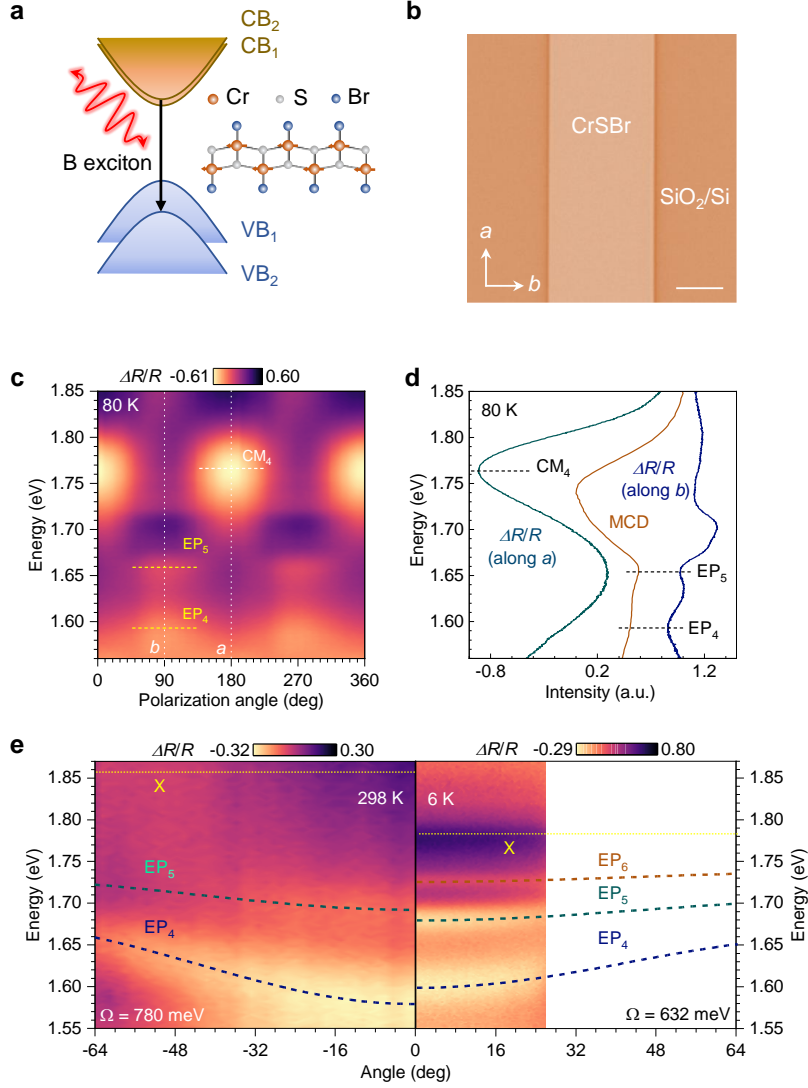


**Figure 1.** (a) Schematic of B exciton transition. (b) Optical image of one CrSBr crystal (thickness of 90 nm) on SiO<sub>2</sub>/Si. White arrows represent the *a*-axis and *b*-axis. Scale bar is 5 μm. (c) Differential reflectance spectra as a function of polarization of reflected light at 80 K under *B* = 1 T. White dashed lines represent polarization along the *a*-axis and *b*-axis. (d) Differential reflectance at 80 K under *B* = 1 T with the polarization of the reflected light along the *a*-axis (cyan) and *b*-axis (navy) and MCD spectrum at 80 K under *B* = 4 T (brown) of the 354 nm-thick CrSBr crystal. (e) Angle-resolved reflectance spectra at 298 K (left panel) and 6 K (right panel) of the 354 nm-thick CrSBr crystal. Dotted curves and dashed curves denote the uncoupled B exciton and lower exciton-polariton branches. The fitted average Rabi splitting energy is 780 meV and 632 meV, respectively.

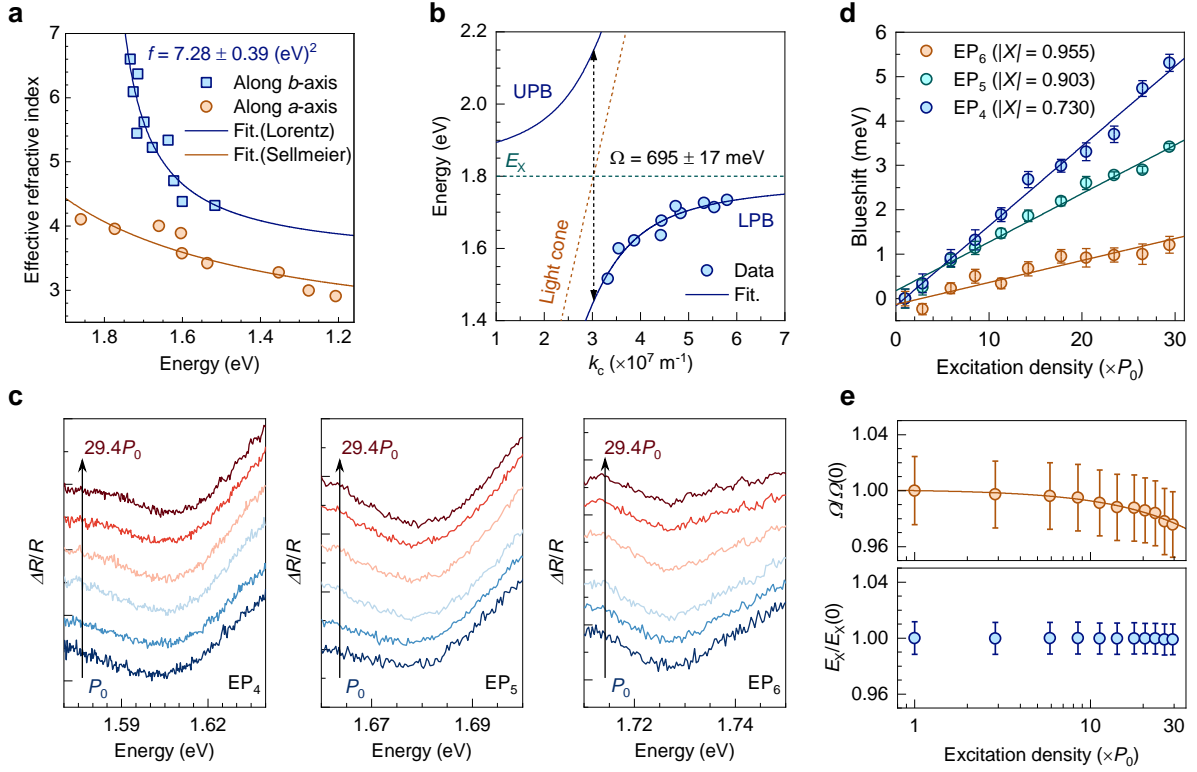


**Figure 2.** (a) Energy dependence of effective refractive index along the  $b$ -axis (navy) and  $a$ -axis (brown). Open circles: experimental data. Solid curves: fitting results. (b) Energy-wavevector dispersion of CrSBr crystals with different thicknesses. Dots: experimental data at normal incidence. Solid curves: fitting results using coupled harmonic oscillator model, giving an average Rabi splitting energy of 695 meV. UPB(LP) stands for the upper(lower) polariton branch. (c, d) Excitation density dependence of reflectance spectra (c) and blueshift (d) for three exciton-polariton branches in the 354 nm-thick CrSBr crystal. Excitation density  $P_0 = 1.25 \times 10^{11} \text{ cm}^{-2}$ . (e) Fitted Rabi splitting energy (upper panel) and B exciton energy (lower panel) relative to the Rabi splitting and B exciton energy obtained at the lowest excitation density as a function of excitation density according to (c).

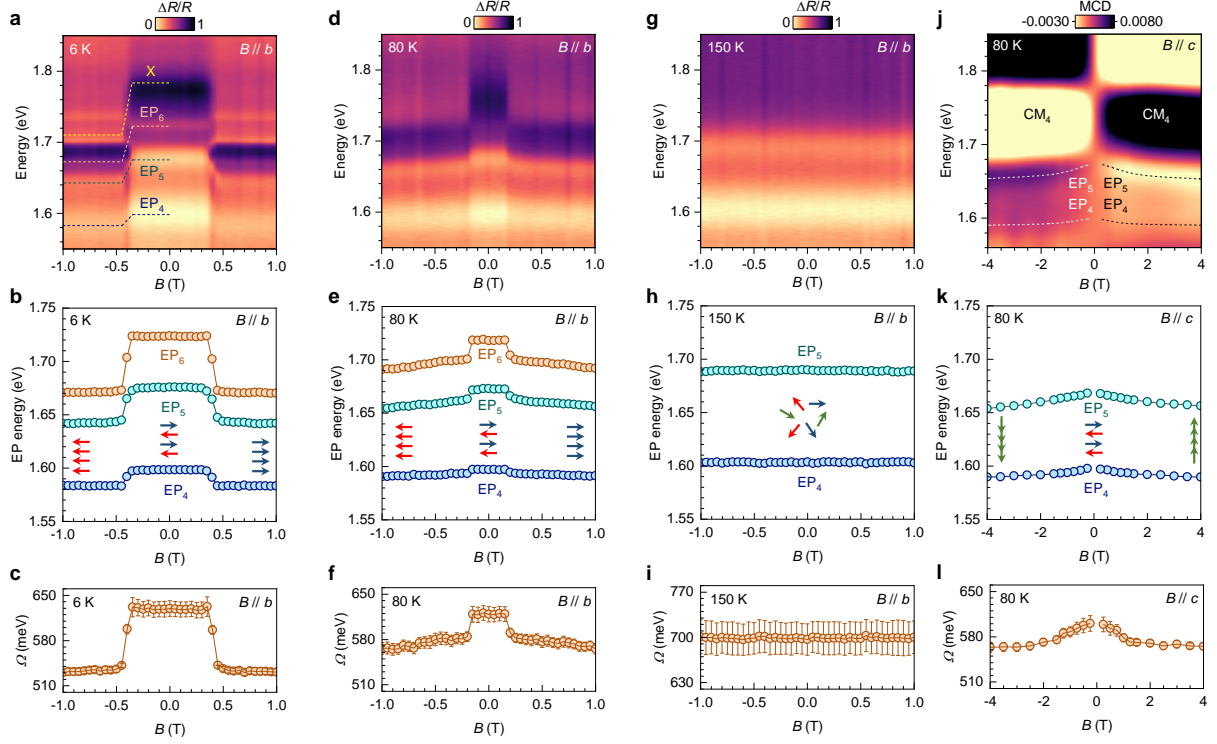


**Figure 3.** (a, d, g, j) Magnetic field dependence of differential reflectance spectra at 6 K (a), 80 K (d), 150 K (g) and MCD spectra at 80 K (j) of the 354 nm-thick CrSBr crystal. (b, e, h, k) Magnetic field dependence of extracted exciton-polariton energies. (c, f, i, l) Magnetic field dependence of fitted Rabi splitting energies. Colored arrows show the possible orientation of magnetizations.

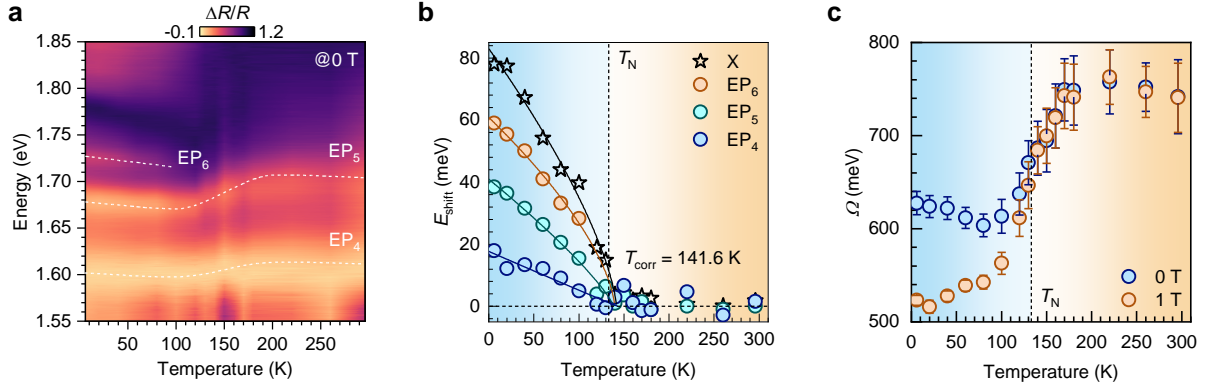


**Figure 4.** (a) 2D colored reflectance spectra at normal incidence of the 354 nm-thick CrSBr crystal at 0 T. The exciton-polariton energies are guided by white dashed curves. (b) Temperature dependence of  $E_{\text{shift}}$  for three exciton-polariton branches and B exciton. The thick curves with corresponding colors are fitting results. (c) Temperature dependence of Rabi splitting energy under  $B = 0$  T (navy) and  $B = 1$  T (brown). The dashed lines in (b) and (c) represent the Néel temperature.